Biol Cybern (2005)
DOI 10.1007/s00422-005-0558-y

ORIGINAL PAPER

Biological Cybernetics

Collins G. Assisi · Viktor K. Jirsa · J. A. Scott Kelso

Dynamics of multifrequency coordination using parametric driving: theory and experiment

Received: 17 June 2003 / Accepted: 18 March 2005 / Published online: 30 May 2005

Abstract The coupling of movement behavior and environmental signals has been extensively studied within the domain of rhythmic coordination tasks. However, in contrast to most traditional coordination studies, here we drive the coupled sensorimotor system far beyond the frequency regime in which these signals may be synchronized. Our goal is to identify the properties of the coupling between the human subject and the environment. Earlier studies have shown that the environmental signal may be parametrically coupled to the effectors. A necessary feature of parametrically driven oscillators is the existence of stable 1:1 and 1:2 coordination modes. Here, we test this prediction experimentally using a coordination paradigm in which subjects were asked to coincide peak finger flexion with an auditory metronome beat. The rate of the metronome was increased in steps of 0.5 Hz from 2.5 Hz to 12 Hz. It was observed that the subjects shifted involuntarily from a 1:1 to a 1:2 coordination mode at high driving frequencies, as predicted. These results are examined in the context of an extended form of the Haken–Kelso–Bunz (Haken et al. 1985) model (HKB) for bimanual coordination, which includes a parametric driving term (Jirsa et al. 2000). Unimanual coordination is treated as a special case of this extended model. An important feature of the HKB model is bistability and the presence of a phase transition from an anti-phase mode to in-phase mode of coordination. Our description of unimanual coordination leads to a mechanism for phase transitions that is distinct from that seen in the HKB model. The transition is mediated by the dynamics of both the amplitude and the phase of the oscillator. More generally, we propose the existence of two types of transitions in our extended theory, that is, phase-mediated and amplitude-mediated transitions. Both have characteristic features; in particular, their transients are mutually orthogonal in the plane spanned by the amplitude and phase of the oscillator. The analytical and numerical results of our theoretical model are demonstrated to compare favorably with our experimental results.

C.G. Assisi · V.K. Jirsa (✉) · J.A. Scott Kelso
Center for Complex Systems and Brain Sciences,
Florida Atlantic University, 777, Glades Road, Boca Raton,
FL 33431, USA
Tel.: +561-2972230
E-mail: jirsa@ccs.fau.edu

1 Introduction

The coordination of movements in humans and animals may be viewed as ordered spatiotemporal structures that arise in a system consisting of a large number of components and processes organized over different spatial and temporal scales (Kelso et al. 1986; Schöner and Kelso 1988a). The behavior of the individual components of the system and the spatiotemporal patterns observed at a macroscopic level of description are linked, using the concepts of synergetics, by means of a few observables known as order parameters. These order parameters in turn govern the dynamics at the microscopic level (Haken 1983). Over the past two decades or so, using concepts from synergetics and the mathematical tools of nonlinear dynamics, a number of studies have addressed various aspects of the dynamics of coordination, especially rhythmic coordination. Rhythmic movements are archetypes of time-dependent behavior in nature. In studies of rhythmic coordination, the elements of the system are often modelled using coupled limit cycle oscillators (Haken et al. 1985; Kelso et al. 1981; Yamanishi et al. 1980; Yuasa and Ito 1990). External stimuli play an active role in the dynamics of such limit cycle oscillator systems. Examples range from firefly entrainment (Buck and Buck 1976) to gait transitions in animals (Collins and Stewart 1993; Schöner et al. 1990). In the context of biological systems, especially in the area of movement coordination, these can be seen as patterns generated by an action-perception system (Kelso et al. 1990).

One of the first oscillator models of coordination behavior is the HKB model (Haken et al. 1985). This model provides a description of experimentally observed bistability and phase transitions in bimanual coordination experiments (Kelso 1984). In these experiments, subjects were asked to move their index fingers rhythmically in opposite phases (involving simultaneous activation of the flexor and extensor

muscles) in time with a metronome. The frequency of the metronome was progressively increased. At a threshold frequency, subjects exhibited a spontaneous transition to an in-phase mode of coordination (simultaneous activation of homologous muscle groups). Such transitions have also been noted in a number of other coordination situations and provide a mechanism that affords the system alternate coordination strategies under changing environmental conditions. Because most of the degrees of freedom of a dynamical system are enslaved close to transition points (Haken 1983), the system dynamics becomes low dimensional and hence provides a window into the structure and function of the system. In this paper, we explore different mechanisms that lead to phase transitions in coordination. In recent experiments, Fink et al. (2000) investigated the role of environmental information in the dynamics of bimanual coordination. A central finding that emerged from this study was that external information may serve to stabilize states that would otherwise have switched to more stable modes of coordination. Jirsa et al. (2000) accounted for this effect by coupling the external information parametrically to a set of limit cycle oscillators. The main idea elucidated by the above studies is that perception and action, environmental information and the dynamics of movement are inextricably linked (Kelso et al. 1990). In this paper, we present an experimental strategy to further examine the assumption that action and perception are parametrically coupled. Further, based on previous models (Haken et al. 1985; Jirsa et al. 2000; Kay and Warren 2001; Kelso et al. 1990; Kay and Warren 1998), we derive a theoretical model for unimanual coordination and compare the features of this model with the observed data.

2 Background and motivation

In order to understand the dynamics of the sensorimotor system, the following elements must be specified.

1. The dynamics of the uncoupled movement system. After (Schöner and Kelso 1988a,b,c), we refer to this as the *intrinsic dynamics*. For our specific experiment, the intrinsic dynamics comprises the rhythmic movement of the finger without reference to the metronome. A number of theoretical and experimental studies have addressed the issue of intrinsic dynamics in different coordination situations. Rhythmic movement of the end effector has been mapped onto the limit cycle of autonomous nonlinear oscillators (Kay et al. 1987). This captures the experimental features of reproducible frequency–amplitude–velocity relationships. Kay et al. (1987) have demonstrated the stability of human rhythmic movements through perturbation experiments. Based on these studies, a concrete limit cycle model can be formulated.
2. The environmental signal, here a rhythmic metronome. This is operationalized in the present theoretical model using a sinusoidally varying function of time.
3. The coupling between the external stimulus and the movement system. This has been variously described using linear (Schöner and Kelso 1988b,c) and parametric terms (Jirsa et al. 2000; Kay and Warren 1998) to drive the limit cycle oscillator. In what follows, we will argue that given the hypothesis of a limit cycle model and a periodic external signal, a linear driving is insufficient to characterize the dynamics of the system, i.e. the driver must be coupled to the system by higher-order terms.

As in Kelso et al. (1990), the present approach is based on a model of bimanual coordination proposed by Haken, Kelso and Bunz in 1985 (Haken et al. (1985)). The so-called HKB model consists of two limit cycle oscillators coupled to each other via a nonlinear coupling term. The equations of motion read,

$$\ddot{x}_i + (\tilde{A}x_i^2 + B\dot{x}_i^2 - \tilde{\gamma})\dot{x}_i + \omega^2 x_i = f_i(x_1, x_2, \dot{x}_1, \dot{x}_2)\,, \quad (1)$$

where,

$$f_1(x_1, x_2, \dot{x}_1, \dot{x}_2) = (\dot{x}_1 - \dot{x}_2)(\alpha + \beta(x_1 - x_2)^2) \quad (2)$$

$$f_2(x_1, x_2, \dot{x}_1, \dot{x}_2) = (\dot{x}_2 - \dot{x}_1)(\alpha + \beta(x_1 - x_2)^2)\,. \quad (3)$$

x_1 and x_2 represent the movement of the fingers. The system is symmetric under exchange of x_1 and x_2. The left-hand side consists of a linear self-excitation, $\gamma\dot{x}$, a Van der Pol term, $x^2\dot{x}$, and a Rayleigh term, $\dot{x}^3$, for saturation. These competing influences define the functional form of the oscillator. The right-hand side consists of a nonlinear coupling term depending on x_1, x_2, and their temporal derivatives. Equations (1, 2, 3) can be reduced to their steady-state amplitude and an equation describing the dynamics of the relative phase, $\phi_1 - \phi_2$ (Haken et al. 1985), where ϕ_1 and ϕ_2 are the phases corresponding to x_1 and x_2, respectively. The amplitude terms are adiabatically eliminated by assuming that the dynamics acts on a time scale much faster than that of the phase variable. The system can then be described by specifying the steady-state amplitude, r, and an equation governing the order parameter dynamics; here, the dynamics of the relative phase, ϕ,

$$r^2 = \frac{\tilde{\gamma}}{\tilde{A} + 3B\omega^2} \quad (4)$$

$$\dot{\phi} = -a\sin\phi - 2b\sin 2\phi\,, \quad (5)$$

where, a and b are constants depending on α, β, and γ. The phase Eq. (5) has fixed points at 0 and π corresponding to in-phase and anti-phase modes of coordination seen in the experiment. On increasing the frequency of movement, ω, the anti-phase state becomes unstable through a reverse pitchfork bifurcation. Beyond a threshold frequency given by,

$$\omega_c = \sqrt{\frac{4\tilde{\gamma}\beta + \alpha\tilde{A}}{-3\alpha B}}\,, \quad (6)$$

the only stable fixed point corresponds to the in-phase mode of coordination. This is in complete agreement with experimental results. In Sect. 6, we will present examples of situations where an adiabatic elimination of the amplitude is not possible, and consequently, show the existence of two routes via which a transition in the phase can take place. Notice, in Eqs. (1, 2, 3) the metronome makes only a non-specific contribution to the dynamics of the system, moving the system

through various coordinative states via a change in ω, without actively participating in the dynamics. The HKB model does not account for the presence of the metronome and in its original form can be described as a model for the intrinsic dynamics of the system. Recent experiments by Fink et al. (2000) and Byblow et al. (1994) have established that the metronome can modify the trajectories of movement. Further, Fink et al. (2000) demonstrated that the presence of the metronome causes not only local changes in the trajectory of movement but also introduces global effects to the dynamics, such as a shift of the critical frequency at which a phase transition from anti-phase to in-phase modes of coordination takes place. The local changes effected by the metronome, in the context of unimanual movement coordination, will be addressed in subsequent sections.

In light of these experiments, it becomes crucial to include the metronome in (1). The HKB model correctly reproduces a number of experimentally observed phenomena including phase transitions, hysteresis (Kelso 1984), critical fluctuations (Kelso et al. 1986) and critical slowing down (Scholz et al. 1987) among others. Hence, it is prudent to retain the HKB model at the core of other models that include environmental influences in a description of the dynamics of unimanual (Kelso et al. 1990) and bimanual coordination. For the latter, this was achieved by Schöner and Kelso (1988b) and Jirsa et al. (2000). Schöner and Kelso (1988b) used an additive linear driving term to describe the effect of the metronome. The environmental information was introduced as an additional force acting on the order parameter, ϕ, dynamics attracting it to the phase of the metronome Schöner and Kelso (1988c). In order to account for the results of Fink et al.'s (2000) recent experiments, Jirsa et al. (2000) used a parametric driving term to describe the effect of the metronome. In the limit of negligible coupling to the metronome, both these models reduce to the original HKB equations. Using equations of motion proposed by Jirsa et al. (2000), the coupling function becomes

$$f_1(x_1, x_2, \dot{x}_1, \dot{x}_2, \epsilon_1, \epsilon_2) = (\dot{x}_1 - \dot{x}_2) \times(\alpha + \beta(x_1 - x_2)^2) + \epsilon_1 \cos\ \tilde{\Omega}t + \epsilon_2 x_1 \cos\ \tilde{\Omega}t \qquad (7)$$

$$f_2(x_1, x_2, \dot{x}_1, \dot{x}_2, \epsilon_1, \epsilon_2) = (\dot{x}_2 - \dot{x}_1) \times(\alpha + \beta(x_1 - x_2)^2) + \epsilon_1 \cos\ \tilde{\Omega}t + \epsilon_2 x_2 \cos\ \tilde{\Omega}t\,, \qquad (8)$$

where ω is the frequency of the finger movement in (1), and $\tilde{\Omega}$ is the frequency at which the metronome is presented. ϵ_1 and ϵ_2 are the strengths of the linear and the parametric coupling terms, respectively. In our description of unimanual coordination, we will use (7, 8). We make the following assumption. The movement of one finger in response to a metronome can be modelled by setting the movement amplitude in one of the oscillators from (7, 8) to zero. The equation of motion of a single finger performing rhythmic movement with a metronome can now be written as follows,

$$\ddot{x}_1 + (Ax_1^2 + B\dot{x}_1^2 - \gamma)\dot{x}_1 + \omega^2 x_1 = \epsilon_1 \cos\ \tilde{\Omega}t + \epsilon_2 x_1 \cos\ \tilde{\Omega}t\,, \qquad (9)$$

where

$$A = \tilde{A} - \beta, \quad \gamma = \tilde{\gamma} - \alpha\,. \qquad (10)$$

The crucial element here is the presence of a parametric driving term. Parametric driving leads to characteristic properties of the $\epsilon_2 - \tilde{\Omega}$ parameter space. The parameter space can be divided into stability and instability regions as shown in Fig. 1.

The frequency of the metronome is plotted along the x-axis and the strength of the parametric coupling term is shown along the y-axis. The lighter regions indicate points in the parameter space where an oscillatory state of a given frequency, that is initially of small amplitude, will grow exponentially. These regions, known as Arnol'd tongues, correspond to coordinative states where the movement of the finger is phase and frequency locked to that of the metronome. Each Arnol'd tongue corresponds to a particular frequency ratio. In the wider tongue, marked 1:2, the frequency of the finger, ω, is subharmonically entrained to the frequency of the metronome, $\tilde{\Omega}$, that is, the oscillator completes one cycle for two cycles of the metronome. In the 1:1 tongue, both the oscillator and the driver have the same frequency. Stable $\omega : \tilde{\Omega}$ (Finger frequency: metronome frequency) coordination modes are obtained for the following frequency ratios (Jirsa et al. 2000).

$$\frac{\omega}{\tilde{\Omega}} = k, \quad k = \frac{1}{2}, 1, \frac{3}{2}, ... \qquad (11)$$

Earlier experiments have studied the dynamics of multifrequency coordination (Kelso et al. 1991; Treffner and Turvey 1996; Peper et al. 1995) and theoretical models of bimanual multifrequency coordination exist (DeGuzman and Kelso 1991; Haken et al. 1996). Kay and Warren (1998) have described multifrequency coordination using parametric

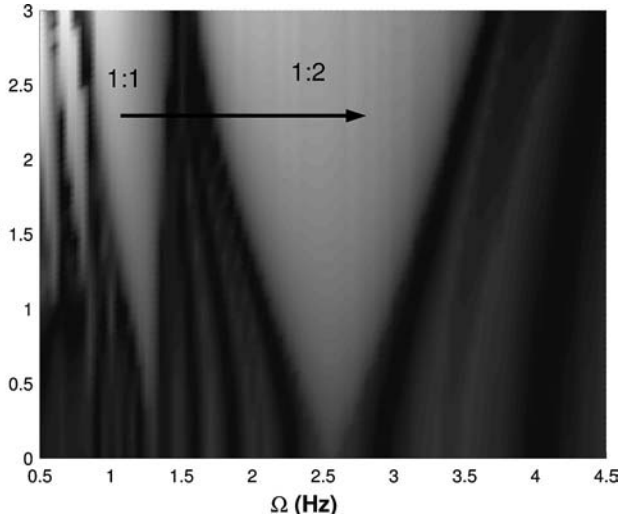

Fig. 1 Plot of the Arnol'd tongue structures seen for the parametrically driven oscillator system described by Eq. (9). Along the x-axis are the frequencies of the driver Ω and along the y-axis are the strengths of the parametric coupling term ϵ_2. The lighter regions are Arnol'd tongues. The widest Arnol'd tongue corresponds to a 1:2 coordination mode. The next widest region is the 1:1 mode. Other modes correspond to $\omega/\Omega = k$, where, $k = 3/2, 2...$ are progressively smaller. In the experiment, we move from the 1:1 to the 1:2 coordination mode as the driving frequency Ω is increased along the arrow shown in the figure

driving to explain the coupling between gait and posture. (see also (Kay and Warren 2001))

The goal of our experiment is to drive the system through different coordination regimes, i.e. different frequency ratios, by increasing the frequency of the metronome along the direction shown in Fig. 1. In order to see frequency and phase locking in the experiment, it is necessary that the Arnol'd tongue structures are wide enough so that the system does not fall into a qualitatively different solution due to tiny perturbations that are inevitable in any biological system. In our model, the broadest Arnol'd tongues correspond to the 1:1 and 1:2 modes of coordination and there are no other stable coordination modes in between. Experimentally and operationally, we refer to these as the single and double metronome conditions, respectively. In the single metronome condition, each cycle of the finger movement corresponds to one cycle of the metronome, whereas in the double metronome condition, each cycle of finger movement corresponds to two cycles of the metronome.

3 Analytical and numerical results

As our starting point, consider (9). For the single metronome condition, we assume $\omega = \tilde{\Omega}$, i.e. the intrinsic frequency of the finger coincides with that of the metronome. For reasons of mathematical convenience, we write, $\tilde{\Omega} = 2\Omega$, that is, Ω is half the metronome frequency. Here, we are interested in solutions that lie within the 1:1 Arnol'd tongue. Consider the following ansatz for the solutions,

$$x(t) = A_0(t) + A_1(t)\mathrm{e}^{2i\Omega t} + A_1(t)^*\mathrm{e}^{-2i\Omega t} \tag{12}$$

The oscillatory system evolves along a closed curve in a two-dimensional phase space. The shifts in the center of mass of the closed curve are described by a time-dependent real quantity, A_0. A_1 and A_1^* are time-dependent complex quantities that can further be split into a real amplitude, $r \in \Re$, and phase, $0 \leq \phi < 2\pi$, as follows,

$$A_1(t) = r(t)\mathrm{e}^{i\phi(t)} \quad A_1^*(t) = r(t)\mathrm{e}^{-i\phi(t)} \tag{13}$$

As a first approximation, we can identify two relevant time scales, a fast time scale corresponding to the frequency of the metronome, $1/2\Omega$, and a slow time scale corresponding to the dynamics of the variables, $r(t)$ and $\phi(t)$. Hence, using the slowly varying amplitude approximation, $|\dot{A}| << 2\Omega|A|$, we obtain the following equations for the derivatives of (12),

$$\dot{x} = 2i\Omega\mathrm{e}^{2i\Omega t} + c.c\,, \tag{14}$$

and

$$\ddot{x} = (4i\Omega\dot{A}_1 - 4\Omega^2 A_1)\mathrm{e}^{2i\Omega t} + c.c\,. \tag{15}$$

Inserting (12, 14, 15) into (9), we obtain terms of the form

$$\mathrm{e}^{2i\Omega t}, \mathrm{e}^{-2i\Omega t} \tag{16}$$

and

$$\mathrm{e}^{6i\Omega t}, \mathrm{e}^{-6i\Omega t}\,. \tag{17}$$

Contributions from (17) are negligible due to the rotating wave approximation (Haken 1983).

By adiabatic elimination, $A_0(t)$ can be expressed in terms of $A_1(t)$ and $A_1^*(t)$.

$$A_0 = \frac{\epsilon_2}{2\omega^2}(A_1 + A_1^*) \tag{18}$$

Using these approximations and with the substitutions (12, 13, 14, 15) in (9), we obtain the following equations for the amplitude and phase of the system,

$$\dot{r} = \left(\frac{\gamma}{2} - \frac{\epsilon_2}{8\omega^2\Omega}\sin\ 2\phi\right) r - \left\{\frac{3}{2}\alpha\Omega^2 + \frac{\beta}{2} + \frac{\beta\epsilon_2}{4\omega^4} (\cos 2\phi + 1)\right\} r^3 - \frac{\epsilon_1}{4\Omega}\sin\ \phi\,, \tag{19}$$

and

$$\dot{\phi} = \frac{\omega^2 - 4\Omega^2}{4\Omega} - \frac{\epsilon_1}{8\Omega r}\cos\ \phi - \frac{\epsilon_2^2}{16\Omega\omega^2}(\cos\ 2\phi + 1)\,. \tag{20}$$

Equation (20) for the phase consists of contributions from linear and parametric driving terms. In order to simplify the analysis, we assume that the contribution from the linear driving term is negligible, that is, $\epsilon_1 << \epsilon_2$, and $r \neq 0$ because the linear term enforces monostability (see Jirsa et al. (2000)). In this section, we consider a situation in which the system is far from a phase transition. A complete description is provided in Sect. 6. The steady-state value for the phase, ϕ, is governed by the following equation,

$$\cos\ 2\phi = \frac{4(\omega^2 - 4\Omega^2)\omega^2 - \epsilon_2^2}{\epsilon_2^2}\,, \tag{21}$$

which has two steady states corresponding to synchrony of the metronome with peak flexion or peak extension. In order to destabilize one of the solutions, we require a contribution from the linear driving term. In our approximation, we set $\epsilon_1 = 0$, thus neglecting the contribution from the linear driving. In Sect. 6, we will elaborate on the different mechanisms of phase transitions when $\epsilon_1 \neq 0$. Note that our experiment is not designed to test this prediction explicitly, which is open to future experimentation. Using (21) in (19), we obtain a cubic equation of the form

$$Ar - Br^3 = 0\,, \tag{22}$$

where the coefficients, A and B, are given by,

$$A = \frac{\gamma}{2} - \frac{1}{8\omega\Omega}\sqrt{2(\omega^2 - 4\Omega^2)(\epsilon_2^2 - 2(\omega^2 - 4\Omega^2)\omega^2)} \tag{23}$$

and

$$B = 12\alpha\Omega^2 + \frac{\beta}{2} + \frac{\beta}{\omega^2(\omega^2 - 4\Omega^2)}\,. \tag{24}$$

The amplitude is given by

$$r = \sqrt{\frac{A}{B}} \tag{25}$$

Figure 2 shows the amplitude response to a change in the frequency of the environmental stimulus ($\tilde{\Omega}$) that drives the

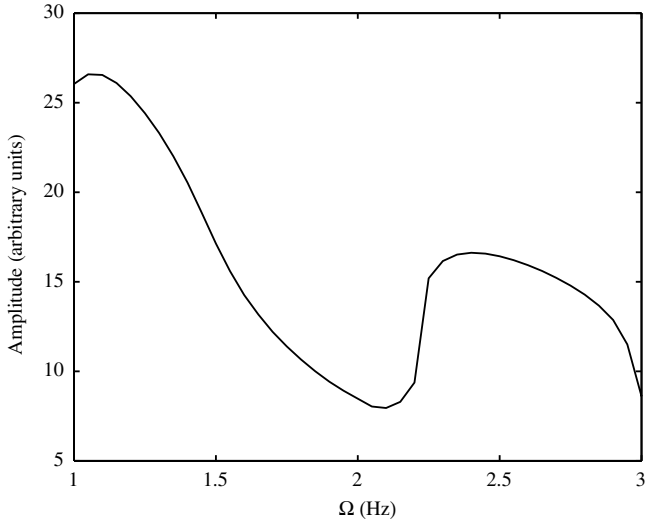

Fig. 2 Plot of the amplitude associated with the most dominant frequency of the oscillator ω as the frequency of the driver $\tilde{\Omega}$ is increased. The nonmonotonic behavior of the curve is characteristic of the resonance structure of the oscillator system

oscillator, obtained by integrating Eq. 9 for different values of $\tilde{\Omega}$. The spectral power was computed using a discrete Fourier transform on the steady-state time series associated with a particular driving frequency. As the frequency is increased, the system moves through the parameter space from the 1:1 to the 1:2 Arnol'd tongue along the line, as shown in Fig. 1. Within an Arnol'd tongue structure, the amplitude shows an inverted U-shaped dependence with increasing driving frequency. Such nonmonotonic behavior originates due to the finite width of theArnol'd tongue.

3.1 Double metronome condition

Here, we seek solutions such that $\omega = \tilde{\Omega}/2 = \Omega$, i.e. the frequency of finger movement is one half that of the metronome. We use the following ansatz for the solutions within the 1:2 Arnol'd tongue,

$$x(t) = A_1 e^{i\Omega t} + A_1^* e^{-i\Omega t} . \tag{26}$$

The analysis follows the lines of the single metronome condition. As before, A_1 and A_1^* are time-dependent coefficients that can be split into amplitude and phase components.

$$A_1(t) = r(t)e^{i\phi(t)} \quad A_1^*(t) = r(t)e^{-i\phi(t)} \tag{27}$$

Performing the slowly varying amplitude and rotating wave approximations, with (26, 27) in (9), we obtain the following equations for the amplitude and phase of the oscillator,

$$\dot{r} = \left(-\frac{3}{2}\alpha\Omega^2 + \frac{\beta}{2}\right) r^3 + \left(\frac{\gamma}{2} - \frac{\epsilon_2}{4\Omega} \sin\ 2\phi\right) r \tag{28}$$

and

$$\dot{\phi} = \frac{\omega^2 - \Omega^2}{2\Omega} - \frac{\epsilon_2}{4\Omega} \cos\ 2\phi . \tag{29}$$

Considering the steady-state solutions of (28) and (29), we have for ϕ

$$\cos\ 2\phi = \frac{2(\omega^2 - \Omega^2)}{\epsilon_2} . \tag{30}$$

Replacing this in (28), we obtain an equation describing the steady-state amplitude.

$$Ar - Br^3 = 0 \tag{31}$$

where,

$$A = \frac{\gamma}{2} - \frac{1}{4\Omega}\sqrt{\epsilon_2^2 - 4(\omega^2 - \Omega^2)^2} \tag{32}$$

and

$$B = \frac{3}{2}\alpha\Omega^2 + \frac{\beta}{2} . \tag{33}$$

The steady-state amplitude is given by,

$$r = \sqrt{\frac{A}{B}} . \tag{34}$$

As in the single metronome condition, here too, we observe an inverted U-shaped amplitude dependence. In Fig. 2, the two humps correspond to the single and double metronome condition, respectively.

3.2 Stochastic properties

A characteristic property of all biological systems is the presence of noise, the sources of which are both internal and environmental. The movements are therefore not exactly reproducible across trials or even across cycles of a single trial. In order to account for the variability seen in the experimental data, we must include noise in (9). The simplest way to do this is by using an additive Gaussian noise term, $\xi(t)$, with the following properties.

$$\langle \xi(t) \rangle = 0, \ \ \langle \xi(t)\xi(t+\tau) \rangle = Q^2\delta(\tau), \quad Q = 0.01 \tag{35}$$

Schöner et al. (1986) studied the effects of noise for the case of self-paced bimanual coordination. For a parametrically driven oscillator, the trajectories of motion are asymmetric in phase space. The variability is distinctly lower at points of the trajectory that are coincident with peaks of the external signal than at other points. In Figs. 3a and 3b, we summarize the results of a numerical simulation obtained from adding a Gaussian noise term to (9). Figure 3a describes the single metronome condition for a particular driving frequency. The driving frequency is at the center of the 1:1 Arnol'd tongue (1.2 Hz). The points of peak flexion and extension are marked in the figure. Clearly, the trajectory shows lower variability at peak flexion than at peak extension. This effect can be attributed to the presence of a stimulus at peak flexion which is absent at the opposite reversal point. Figure 3b shows the effect of the stimulus on the trajectories of motion for the double metronome condition. A frequency was chosen at the center of the 1:2 Arnol'd tongue. Here, unlike

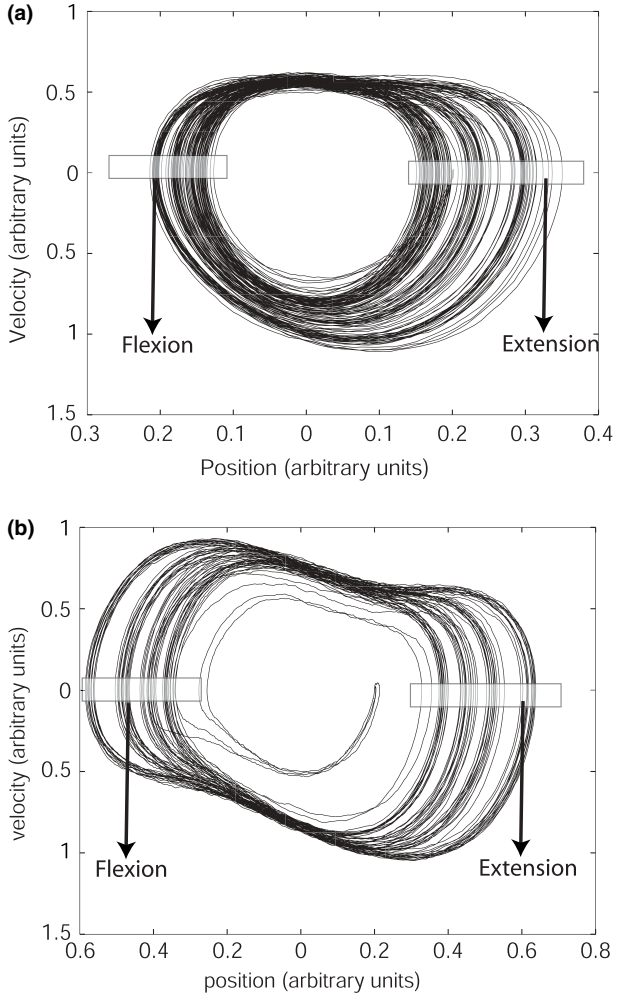

Fig. 3 Phase plane trajectories (position vs. velocity) obtained from Eq. (9) with an additive Gaussian noise term. **a** Single metronome condition: The frequency of the oscillator coincides with the frequency of the metronome. A metronome beat is present only at flexion ($\omega = 2, \tilde{\Omega} = 2$) **b** Double metronome condition: The frequency of the oscillator is half that of the metronome. A metronome beat is present at flexion and extension. ($\omega = 2, \tilde{\Omega} = 4$). The other relevant parameters are $\epsilon_1 = 0.1,\ \epsilon_2 = 3$

in the previous case, Fig. 3a, the trajectories are symmetric in phase space. In the double metronome condition, the environmental stimulus occurs at both peak flexion and peak extension. Hence, the trajectories at the two reversal points show similar variability. A discussion of these results will follow in the next section where we compare the theoretical predictions of the model with our experimental observations.

4 Experiment

In the experiment, subjects moved their index finger back and forth on a parasaggital plane in accord with the frequency of an external metronome. As the frequency of the driver was increased, we expected subjects to move from a 1:1 to a 1:2 mode of coordination after passing through a region of phase drift.

4.1 Participants

Nineteen right-handed subjects (14 male and 5 female aged between 19 and 40 years.) took part in the experiment. Most of the participants were volunteers from an undergraduate class at Florida Atlantic University. All procedures were approved by the local Institutional Review Board for the protection of human subjects and participants signed consent forms before taking part in the experiment.

4.2 Apparatus

Participants placed the index finger of their dominant hand in a custom built manipulandum that restricted the motion of the metacarpophalangeal joint to a single plane (see Kelso and Holt (1980) for a complete description). Unnecessary vertical and horizontal hand movements were restricted by a padding placed against the sides of the hand. An angle calibrated potentiometer situated above the axis of motion was used to measure the position of the index finger. Finger movement was sampled at 128 Hz using an ODAU analog-digital converter connected to an OPTOTRAK 3010 system. The external metronome, consisting of a sequence of comfortably sounding beeps, each of 40-ms duration, was sent to the ODAU unit and a pair of headphones.

4.3 Procedure

Handedness was first determined using the Edinburgh Handedness inventory. During the experiment, the frequency of the metronome was increased from 2.5 Hz to 12 Hz in steps of 0.5 Hz. Thirty cycles of the metronome were presented at each frequency. At the end of each block of 30 cycles, the metronome frequency was stepped up by 0.5 Hz. A single trial consisted of 20 blocks (2.5–12 Hz) that were presented continuously in order of increasing frequency. Each subject performed five trials. Subjects were asked to coincide peak flexion of the index finger of their dominant hand with the onset of the auditory metronome. Since we did not perform a similar task asking subjects to coincide peak extension with the metronome beat, we cannot test for phase transitions from extension to flexion with our present experimental design, although such effects are well known (Kelso 1984). Prior to the start of the experiment, participants were told, "if the initial pattern of movement changes, do not force yourself to go back to it. Just continue with the pattern you find most comfortable".

4.4 Analysis

We first analyzed the metronome signal to find the onset of the beeps. This information was used to divide the movement

data collected over a given trial into frequency plateaus. Each frequency plateau was coincident with a block of thirty metronome beeps. We noted that the finger movement over a given frequency plateau was almost sinusoidal. A discrete Fourier transform was performed and a single dominant frequency was obtained for each frequency plateau. The spectral power associated with other frequencies was relatively small. The most prominent frequency for a given frequency plateau was chosen as the frequency of finger movement, ω, for that plateau.

In order to classify a particular frequency plateau as 1:1 or 1:2, the following classification scheme was used. Let t_P denote the time of occurrence of a local maximum of the finger movement and t_V a local minimum. The time of onset of a metronome beat is denoted by t_M. The cycles in which the patterns or $t_M \leq t_V \leq t_P \leq t_M$ occur were classified as 1:1 coordination cycles. The cycles in which the subjects performed the patterns $t_M \leq t_P \leq t_M \leq t_V$ or $t_M \leq t_V \leq t_M \leq t_P$ were classified as $1:2$ coordination cycles. Examples of cycles that were classified as 1:1 or 1:2 are shown in Figs. 4a and b, respectively. If, during a particular frequency plateau consisting of 30 cycles, more than 80% of the cycles performed by the subject were 1:1 coordination cycles, then the frequency plateau was classified as a 1:1 coordination plateau. Similarly, the 1:2 coordination plateaus consisted of conditions in which more than 80% of the cycles were 1:2 coordination cycles. In our experiment, the task involved a range of metronome frequencies that were significantly higher than is traditionally used in finger movement studies since we were looking for subharmonic entrainment of the finger movement to the metronome. We sampled twenty frequency plateaus per trial. The sequence of metronome frequencies were presented in succession without a break in between frequency plateaus. Due to this experimental design, we were compelled to restrict the number of cycles per trial to 30 so that fatigue would not be a significant issue. However, using merely 30 cycles for higher frequencies implies that the length of each frequency plateau is small (A 5-second plateau for a metronome frequency of 6 Hz and less for higher frequencies). Therefore, our frequency estimate has reduced accuracy with increasing metronome frequency. Hence, a weak ordinal criterion to identify mode locks (if 80% of the cycles in a frequency plateau are 1:1, then the plateau is classified as such) had to be employed. Thus, it cannot be said that a stable mode locking was established.

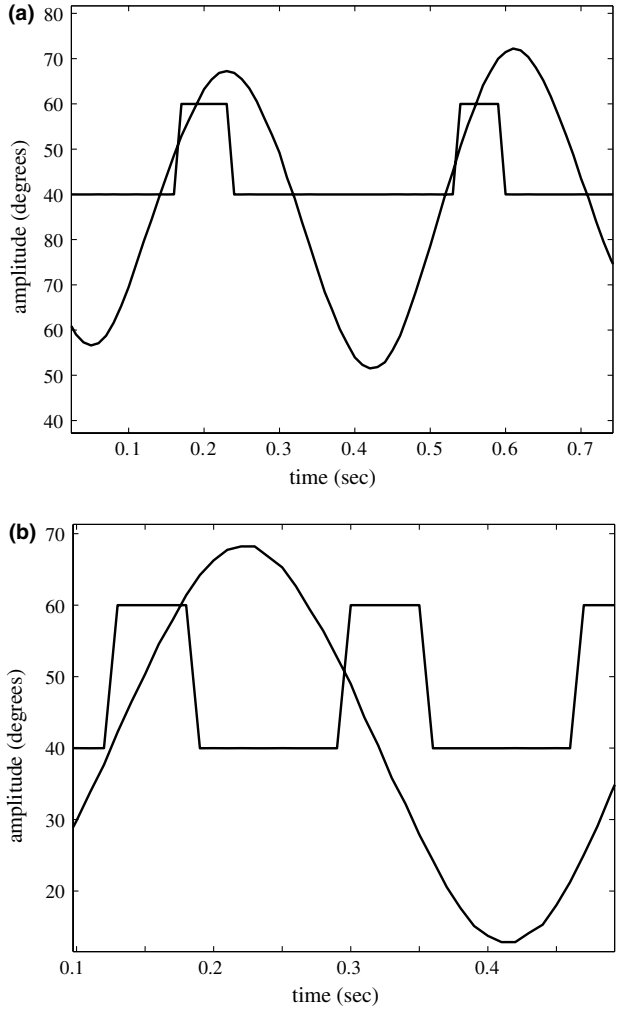

Fig. 4 Classification of coordination patterns. The smooth curves are the trajectories of finger movement and the rectangular pulses represent the metronome. Amplitude is measured in units of the angular displacement (degrees). **a** An example of a pattern that was classified as 1:1 coordination and **b** example of a pattern that was classified as 1:2 coordination. See text for details

5 Results

The results presented in this section will follow the steps in our theoretical analysis. In order to characterize the oscillator system and the coupling between its components, we considered three aspects of the behavior.

1. The frequency of finger movement in relation to that of the metronome.
2. The phase of finger movement at the point of onset of the metronome.
3. The amplitude response for various driving frequencies.

5.1 Frequency

One of the primary goals of this experiment is to determine whether a consistent frequency relationship exists between the metronome and the movement of the subject's index finger. In Figs. 5a, b, c, $\tilde{\Omega}$ is the frequency of the metronome and ω, the frequency of finger movement as defined above. The regions in which the subject maintained a fixed frequency ratio, $\tilde{\Omega}/\omega$, appear as horizontal plateaus in the figure.

Figures 5a, b, c presents the results from three subjects, representative of the broad range of behavioral patterns seen across all nineteen subjects. The ratio of the frequency of the metronome to the frequency of finger movement, $\tilde{\Omega}/\omega$, was

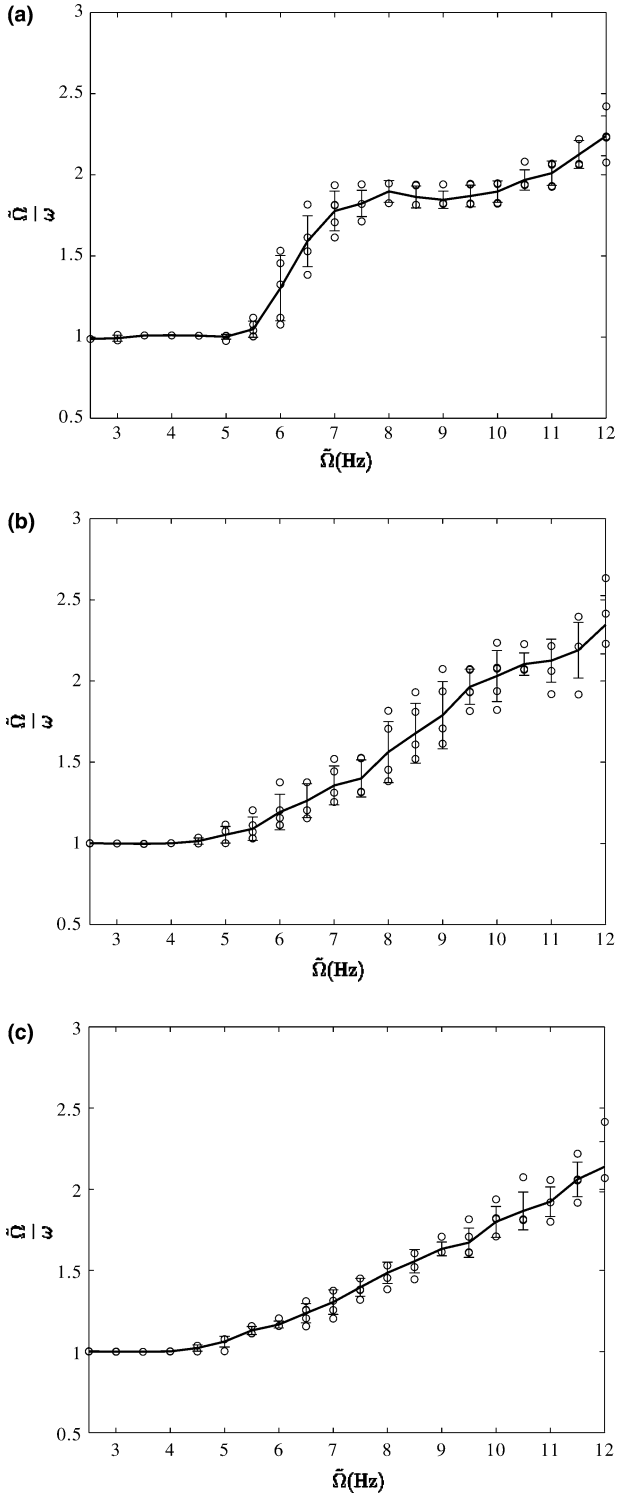

Fig. 5 The *circles* show the frequency ratios for five trials at each frequency plateau, and the bars represent the standard deviation (see text for details). ω is the frequency of finger movement and $\tilde{\Omega}$ is the frequency at which the metronome is presented. The data shown in a, b, and c are from three subjects and are representative of the patterns seen across all nineteen subjects

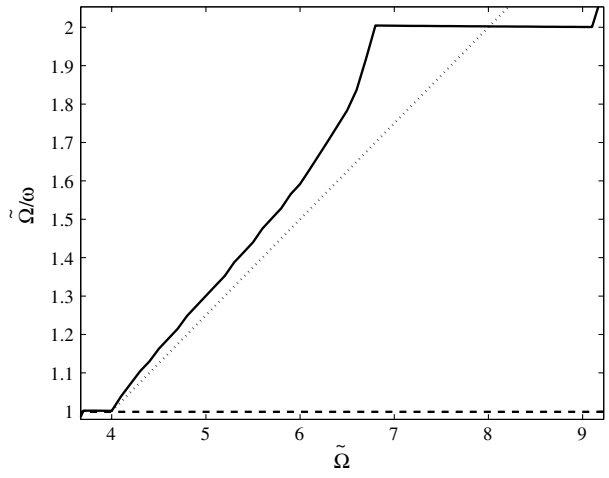

Fig. 6 Plotted are the frequency of the driver Ω versus the ratio Ω/ω for three possible coupling scenarios between stimulus and movement. The *dashed line* represents the profile due to purely linear driving obtained by setting $\epsilon_1 = 0.1$ and $\epsilon_2 = 0$. The *solid line* indicates parametric driving obtained by setting $\epsilon_1 = 0.1$ and $\epsilon_2 = 10$. The *dotted line* shows the behavior of the oscillator which, above a maximum threshold frequency, exhibits a constant frequency of oscillation regardless of the frequency of the driver.The other parameter values are from Eq. 9 are $A = 1.5$; $B = 1$; $\gamma = 0.1$; $\omega = 4$

computed for each frequency plateau. The plotted ratio is the mean of five 30-cycle plateaus with the same frequency for a particular subject. The standard deviation across five trials for each subject is shown as error bars in Fig. 5. Most subjects show a distinct 1:1 mode of coordination followed by a region where the ratio $\tilde{\Omega}/\omega$ does not persist at a constant value. In the 1:2 regime, the behavior varies continuously across subjects, ranging from a strong pattern of frequency locking (Fig. 5a) to no apparent frequency locking (Fig. 5c). Within the context of driven limit cycle oscillators, we consider three possibilities for the type of coupling. These are illustrated in Fig. 6, which was generated by simulating a driven oscillator under different conditions of driving:

1. The coupling between the metronome and the finger is purely linear (Schöner and Kelso 1988c). This is depicted by the dashed line in Fig. 6. A linear coupling implies that the frequency of finger movement always coincides with the frequency of the driver. Hence, we would expect to see only one plateau in the figure, that of 1:1 coordination. This clearly violates the patterns of experimental results observed. Hence, a purely linear driving term is insufficient to explain our experimental findings.
2. The subjects were able to move their finger in a 1:1 pattern until a certain threshold frequency was reached beyond which they maintained a constant frequency. This is depicted by the dotted line in Fig. 6. Here, we assumed that the oscillator performs 1:1 coordination until a threshold frequency of 5 Hz, beyond which a constant frequency

is maintained throughout the range of frequencies of the driver. This compares with the behavior seen in Fig. 5c where the subject performed 1:1 coordination until a frequency of 4.5 Hz and then maintained an almost constant frequency (mean = 5.4 Hz, standard deviation = 0.37) throughout the rest of the trial. However, this possibility alone does not account for the behavior seen in Fig. 5a. Therefore, we must account for another possibility.

3. The coupling between the finger and the external driver is achieved using a parametric driving term. This is depicted in Fig. 6 by the solid line. Here, we see the existence of two plateaus corresponding to a 1:1 and a 1:2 mode of coordination. Compare this with the behavior seen in Fig. 5a. Here, the subject clearly shows the presence of two plateaus corresponding to the 1:1 and 1:2 modes of coordination.

The behavior seen across all 19 subjects can be described in terms of varying contributions from the latter two forms of coupling and can be compared with the theoretical model given by Eq. (9).

Our model predicts that the width of the Arnol'd Tongue structures increases as a function of the strength of the parametric (ϵ_2) driving term. This behavior is plotted as a function of ϵ_2 in Fig. 7 for both plateaus, 1:1 and 1:2. In order to compute the width of each Arnol'd tongue for a particular driving frequency, $\tilde{\Omega}$, we first performed a discrete Fourier transform on the steady-state time series obtained by numerically integrating Eq. 9. The most dominant frequency was then chosen as the frequency of the oscillator, ω. The width of the 1:1 Arnol'd tongue was determined by identifying the points within $|\omega - \tilde{\Omega}| < 0.1$. Similarly, we computed the width of the 1:2 Arnol'd tongue by identifying the points within $|\omega - \frac{\tilde{\Omega}}{2}| < 0.1$

In Figs. 8a, b we describe the broad range of behavior seen across all 19 subjects. Each bar in the figure corresponds to a single subject. The height of the bar represents the number of frequency plateaus in which the subject demonstrated a 1:1 (Fig. 8a) or 1:2 (Fig. 8b) mode of coordination. The procedure identifying the width of a synchronization plateau is described in Sect. 4.4. In Fig. 8, the subjects are arranged in ascending order of the number of frequency plateaus in which each subject showed 1:1 (Fig. 4a) or 1:2 (Fig. 4b) modes of coordination. Here, 14 out of 19 subjects show significant plateaus (as defined in the section 4.4) of at least 1.5 Hz width for 1:1 coordination, whereas 11 out of 19 subjects show plateaus with at least 1.5 Hz width for 1:2 coordination. The variation in the width of the synchronization plateaus (Figs. 8a-b) may indicate a variation in the coupling strength across subjects. The relationship between the coupling strength and the width of the plateaus for our model is shown in Fig. 7.

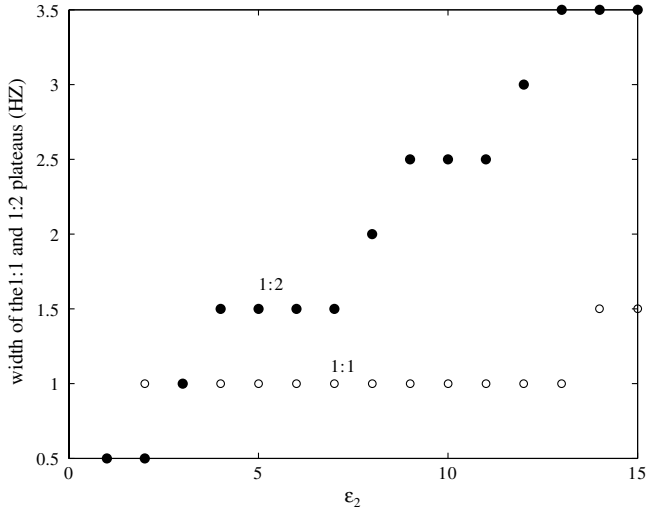

Fig. 7 Plotted is the width of the 1:1 (*empty circles*) and 1:2 (*filled circles*) Arnold tongues as the strength of the parametric coupling term, ϵ_2, is varied. See text for details

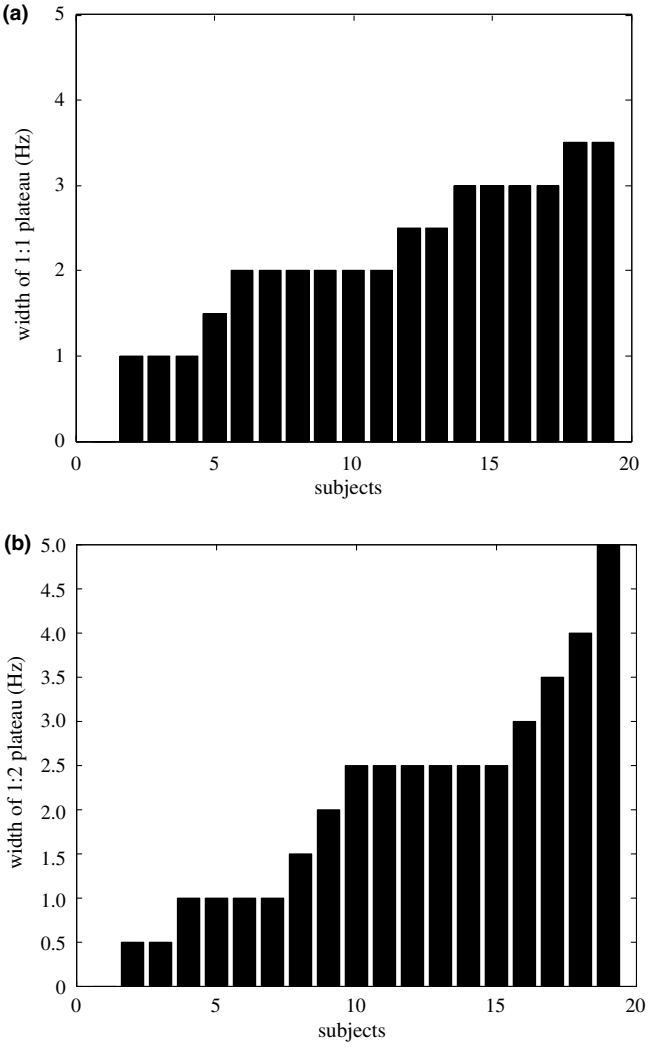

Fig. 8 Each bar corresponds to a subject and the height of the bar corresponds to the width of 1:1 **a** or 1:2 **b** frequency conditions. See text for details

5.2 Amplitude

In this section, we examine two aspects of the dynamics, the amplitude response to a change in frequency and the effect of the metronome on the trajectory of finger movement.

5.2.1 Amplitude–frequency relationship

As mentioned earlier, the movement is almost sinusoidal. Since the frequency variability within a given frequency plateau is small, we may use the spectral power associated with the most dominant frequency as a measure of the amplitude. Spectral power associated with the neighboring frequencies does not cause a qualitative change in the amplitude response function. Figure 9a shows the mean amplitude response to a change in frequency for all 19 subjects. As the frequency of the metronome is increased, the amplitude of finger movement decreases consistently across subjects. Different frequency-amplitude relationships, other than monotonically decreasing, have been observed over limited ranges of the frequency. Kugler and Turvey (1997) described an inverted U-shaped behavior for a bimanual wrist-pendulum system. The existence of a non-monotonic frequency-amplitude relationship has also been shown in single trials by Beek et al. (2002). We found similar frequency-amplitude relationships for some trials although this was quite variable across subjects. In Fig. 9b, for example, the maxima of the amplitude roughly coincide with the different frequency plateaus associated with the 1:1 and 1:2 Arnol'd tongues in Fig. 5a. Both these figures are obtained using data from the same subject. Parametric excitation, as discussed in sections 3.1 and 3.2, provides a straightforward explanation of the amplitude response behavior observed in Fig. 9b. However, the data averaged across subjects and trials show only a monotonic decrease in amplitude (Fig. 9a), and a finer structure that might resolve the peaks in the region associated with the 1:2 Arnol'd tongue cannot be seen.

The experimental condition required subjects to coincide peak flexion with the metronome beat. In frequency regimes where the subjects performed a 1:1 coordination pattern, peak flexion coincided with the metronome. At the opposite reversal point, peak extension, the metronome was absent. Figure 10a was generated using the data from one subject performing in the 1:1 coordination mode at a frequency of 4 Hz. Along the horizontal axis is plotted the position, and along the vertical axis, the velocity of the finger. The boxes show the regions corresponding to maximum flexion and extension in the phase plane. Compare the spread of the trajectories in the box marked 'flexion' with that in the boxmarked 'extension'. The standard deviation is clearly lower (0.19) for peak flexion compared to peak extension (0.40). The phase space trajectory at 8Hz is plotted in Fig. 10b. Here, the subject performed a 1:2 mode of coordination. In the 1:2 mode of coordination, peak flexion and peak extension are coincident with a metronome beat. This trajectory is more symmetric than the one seen in Fig. 10a. In Fig. 10c, the standard deviation of the position of the peaks of finger movement for a particular frequency plateau was first computed and averaged across five trials. The white bars in Fig. 10c show this averaged quantity for a particular subject. The standard deviation of peak extension was similarly computed and represented by the black bars in the figure. The standard deviation at peak flexion for low frequencies (<6 Hz) that correspond to 1:1 modes of coordination is markedly lower than for extension. A t-test was performed at a 95% confidence level. The frequency plateaus where the standard deviation of extension was higher than flexion at this level of significance are marked with an asterisk in Fig. 10c. At higher frequencies (>6 Hz), the standard deviation for flexion and extension do not show a similar relationship. Earlier studies in bimanual coordination experiments have also shown the presence of

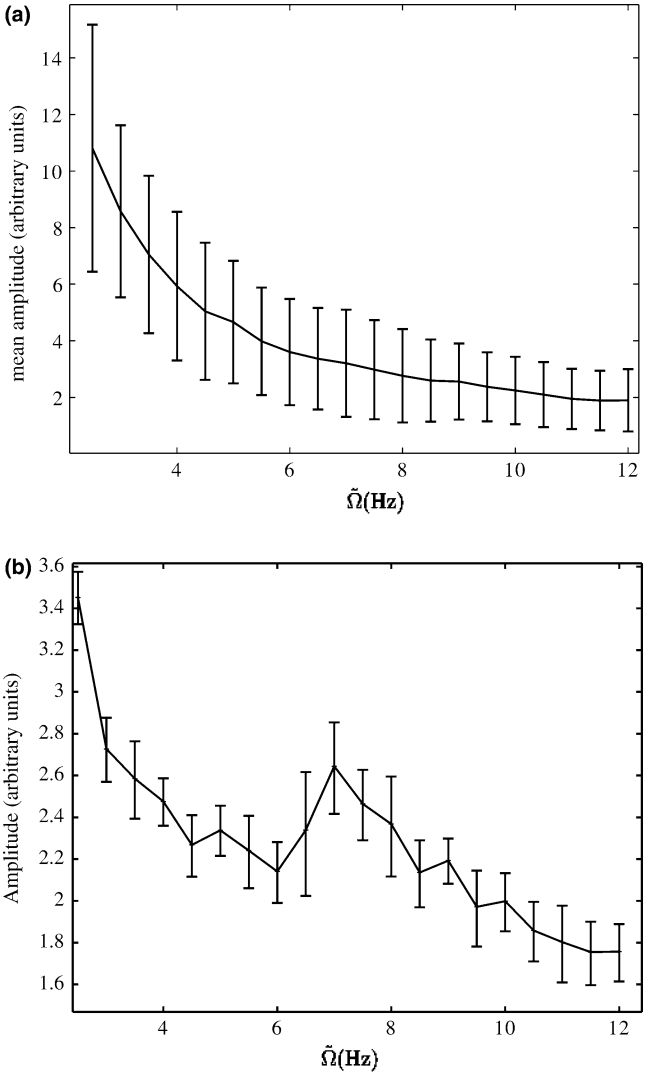

Fig. 9 **a** Plot of the mean amplitude as a function of the frequency of the metronome. The mean is obtained for each frequency plateau using data from 19 subjects. The *error bars* show the standard deviation across 19 subjects for all trials. **b** The data are from one subject and averaged across five trials. Here, we can see the presence of two peaks at 2.5 Hz and 7 Hz. These features may correspond to the positions of the 1:1 and 1:2 Arnol'd tongues

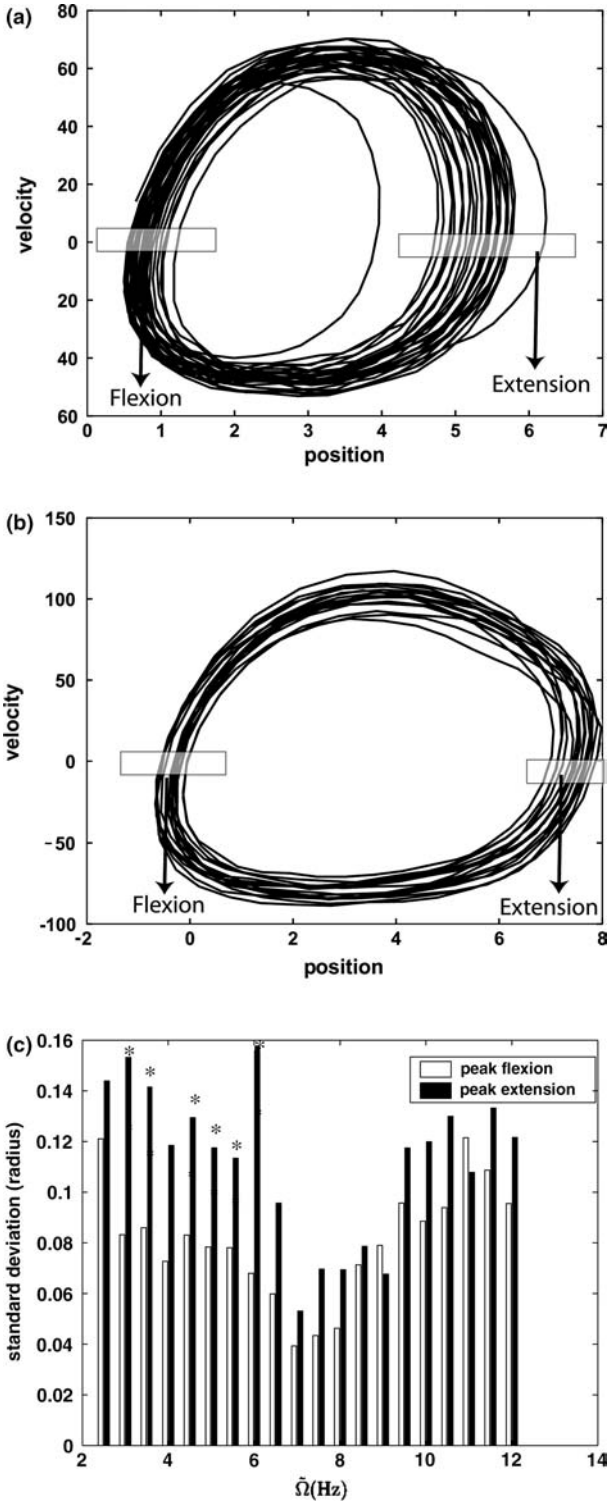

Fig. 10 Experimentally obtained phase plane trajectories of finger movement for one subject at frequencies of 4 and 8 Hz, respectively. The boxes indicate the regions of peak flexion and extension. **a** At 4 Hz (10 A), the subject performs a 1:1 mode of coordination and a metronome beat is coincident with peak flexion. **b** At 8 Hz, the subject performs in a 1:2 coordination mode and the metronome is coincident with both peak flexion and extension. **c** Standard deviation of the points of peak flexion and peak extension are shown. The *white bar* shows peak flexion and the *black bars* show peak extension. Frequency plateaus where the standard deviation of extension is significantly higher than flexion ($p < 0.05$) are marked with an *asterisk*

this phenomenon, referred to in the literature as anchoring (Byblow et al. 1994). Fink et al. (2000) showed that the presence of a metronome at both peak flexion and extension reduces the propensity to switch from an anti-phase to an in-phase mode of coordination as compared to when the metronome is present only at extension. Thus, the presence of specific environmental information affects not only local changes in the trajectory, but also induces changes in the global behavior of the system. The anchoring phenomenon demonstrated in our experimental results compares favorably with that seen in Figs. 3a and b, which was obtained by numerically simulating Eq. (9) in the presence of a Gaussian noise term.

5.3 Phase

The finger movement data for each subject were divided into frequency plateaus using the onset times of the auditory metronome as a reference. We calculated the continuous phase of the movement for each frequency plateau using a Hilbert transform. The points in the continuous-phase trajectory that coincided with the onset times of the metronome were extracted. For each frequency plateau, we obtained 30 such points corresponding to 30 cycles of the metronome. This method of evaluating the phase is equivalent to the commonly used point estimate of the phase for a given cycle, which is usually obtained using the time difference between a peak of finger movement and the onset of the nearest metronome peak. The trace in Fig. 11a shows the standard deviation for each frequency plateau for each trial, averaged across all trials for a given subject. Variability across trials is denoted by the error bars. In Fig. 11b, the driving frequency, $\tilde{\Omega}$, is plotted along the x-axis and the ratio of the driving frequency to the finger movement frequency is shown along the y-axis.

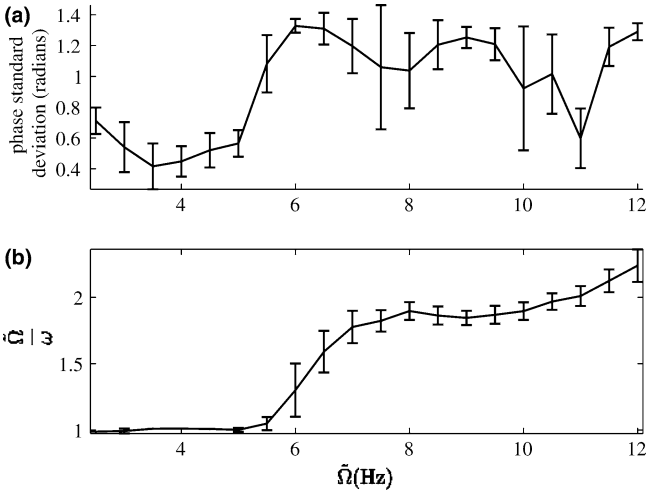

Fig. 11 **a** Standard deviation of the phase of finger movement as a function of the metronome frequency for one subject. *Error bars* represent the deviation of these values across five trials. **b** A plot of the ratio $\frac{\Omega}{\omega}$ versus Ω for the same subject. See text for details

The figure is obtained exactly as in Fig. 5 (see Sect. 5.1). Figures 11a and b are from the same subject and are shown together for comparison.

Figure 12a allows a further exploration of the causes of variability near the borders of Arnol'd tongues. Shown is a section of the time series of the continuous phase strobed using the onset time of the metronome. The segment of the time series shown corresponds to the edge of the 1:1 mode of coordination and the region of phase drift. In the initial part of the time series, the subject performs a 1:1 pattern with respect to the metronome, that is, the onset times of each metronome cycle coincide almost precisely with some phase of the movement cycle. The standard deviation of the phase in this region is small as seen in Fig. 11a. The data in Figs. 11 and 12a, b are from the same subject. As the frequency of the metronome is increased, the subject departs from the 1:1 mode of coordination. (Between 40 s and 55 s in Fig. 12a). This introduces a small frequency difference between the finger movement and the metronome. Each cycle of the metronome strobes the movement at a phase that systematically decreases over the successive cycles, thus introducing a slope in the time series shown in Fig. 12a(between 40 s and 55 s). The rate of the phase drift is proportional to the difference in the frequency. In our experiment, we are constrained to use a maximum of 30 cycles per frequency plateau. Over 30 cycles, the strobed phase is distributed between 0 and 2π. However, due to the small frequency difference, the entire $[0, 2\pi)$ interval does not get covered uniformly in thirty cycles. This is an artifact of the small number of points that are used to sample this interval. A consequence of this non-uniformity at the edge of an Arnol'd tongue is that, across trials, the variability of the phase standard deviation becomes large compared to the variability within an Arnol'd tongue. For higher metronome frequencies in the region of drift, the points of the continuous phase that coincide with the onset of the metronome are distributed uniformly over the interval $[0, 2\pi)$. Therefore, in the drift region the standard deviation across 30 cycles of the metronome is large. However, due to the uniform distribution over the $[0, 2\pi)$ interval, the variability across trials is small. This leads to a maximum in the variability of the standard deviation across trials at the edge of an Arnol'd tongue. Similar maxima are observed at the edge of the 1:2 mode of coordination.

In a small region within the 1:1 coordination mode, the subject showed phase drift and then resumed in a 1:1 mode of coordination. An example is shown in Fig. 12b. This kind of behavior occurs in regions close to the edge of an Arnol'd tongue where a small perturbation, due to intrinsic or environmental noise, plunges the system into a region where the solutions are qualitatively different.

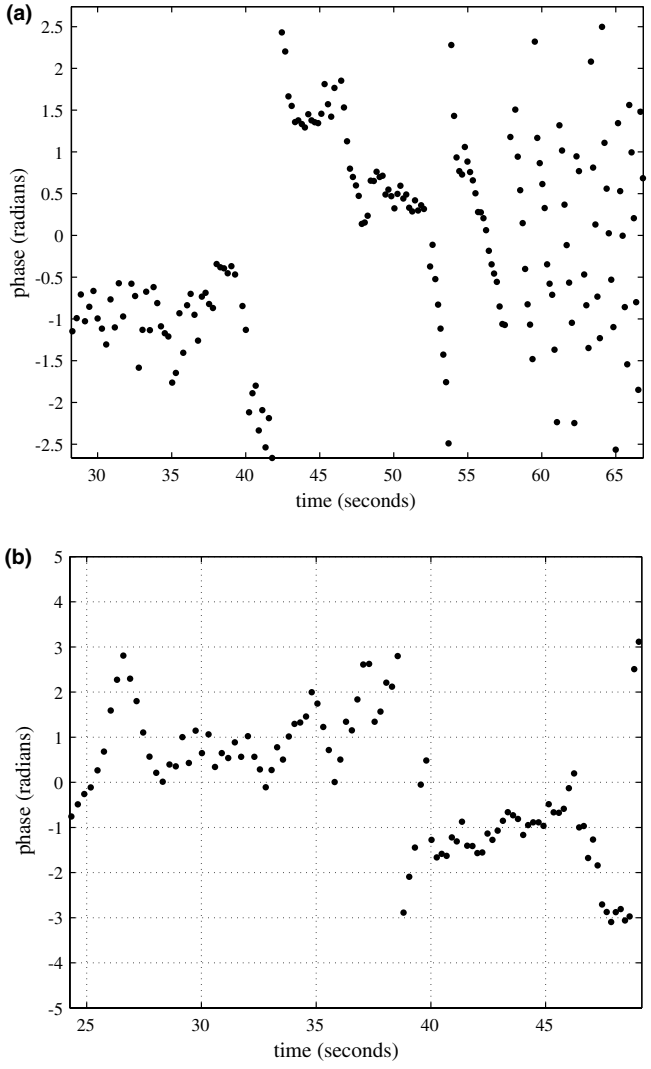

Fig. 12 **a** A plot of the phase of finger movement relative to the stimulus onset for one subject. A segment of the data on the border of the 1:1 mode of coordination is chosen. The behavior shows three distinct regions: a 1:1 coordination mode; a region where the drift is initiated; and a region between the 1:1 and 1:2 modes of coordination. Each point corresponds to the phase associated with one cycle of finger movement. **b** Plot of the phase of finger movement at points of the movement coincident with a metronome beat obtained from a section of the experimental data for one subject. The data shows phase slippages at $t = 35$ s and resetting at $t = 40$ s

6 Mechanisms of phase transitions

One of the crucial features of the HKB model is its ability to characterize the observed phase transitions from anti-phase to in-phase mode of coordination that accompany scalar changes in cycling frequency (Kelso et al. 1981; Kelso 1984). This phenomenon has also been established using more neurally based approaches (Nagashino and Kelso 1992; Grossberg et al. 1997; Jirsa and Haken 1997). Kelso et. al. (1990) have demonstrated a similar transition for the case of a single limb performing a rhythmic coordination task with a metronome. Subjects were asked to perform an off-the-beat rhythmic task, that is, peak flexion was coincident with a point between two metronome beats. As the frequency of movement was increased, subjects spontaneously shifted from an off-the-beat to an on-the-beat pattern of coordination, analogous to a jump

from an anti-phase to an in-phase coordination state seen in bimanual experiments. Research conducted using EEG and MEG (Kelso et al. 1992, 1999; Mayville et al. 2001) has consistently shown that a phase transition in behavior from an anti-phase to an in-phase mode of coordination is accompanied by changes in patterns of neural activity. In this section, we will examine how such a transition can be effected and in the process postulate the existence of two types of transitions, a phase-mediated transition and an amplitude-mediated transition. Consider the equations of motion of the system in the plane spanned by the amplitude, r, and the phase, ϕ.

$$\dot{r} = f(r, \phi), \quad \dot{\phi} = g(r, \phi) \tag{36}$$

The above equations are referred to as the complete system. The complete system may operate on different time scales, for example, the time scale of change in the amplitude variable, r, may be radically different from that of the phase variable, ϕ. The presence of distinct types of transitions arises from a separation of time scales. The faster time scale can be adiabatically eliminated and the slower time scale then dictates the subsequent behavior of the system. For the case of a phase-mediated transition, the amplitude rapidly decays to its steady-state value and the entire dynamics can then be described by the phase variable (Haken 1983).

$$r = f_1(\phi) \quad \dot{\phi} = g(f_1(\phi), \phi) \tag{37}$$

The HKB model is an example of a system that exhibits a phase-mediated transition (Haken et al. 1985). Adiabatically eliminating the amplitude, we arrive at Eqs. (4, 5) for the dynamics. The numerically generated time series in Fig. 13a shows that the transition takes place over a few cycles without any change in the amplitude.

For the case of an amplitude-mediated transition, the dynamics of the phase takes place at a time scale much faster than that of the amplitude. The steady-state value of the phase can now be replaced in the amplitude equation to obtain the entire dynamics of the system.

$$\dot{r} = f(r, g_1(\phi)) \quad \phi = g_1(r) \tag{38}$$

An example of an amplitude-mediated transition is seen in the equations for a parametrically paced version of the HKB oscillators. Transitions in coordination are usually described in polar coordinates, where the relative phase jumps through π and the amplitudes are positive. Alternatively, the phase can be held constant while the amplitude crosses over to a negative value. This description has been advanced by Jirsa et al. (2000). The time series shown in Fig. 13b was obtained by numerically simulating Eq. (9). A phase transition is achieved through an amplitude-mediated mechanism where the amplitude of the oscillation dies down and comes up again in the opposite phase.

Figure 14 illustrates the two different mechanisms for phase transitions. Along the horizontal axis is plotted the phase of the oscillator. The amplitude, r, is plotted along the vertical axis. In a phase-mediated transition, described by Eq. (37), the amplitude remains constant while the phase performs a transition through π. In an amplitude-mediated transition (38), the amplitude decreases and then grows, but

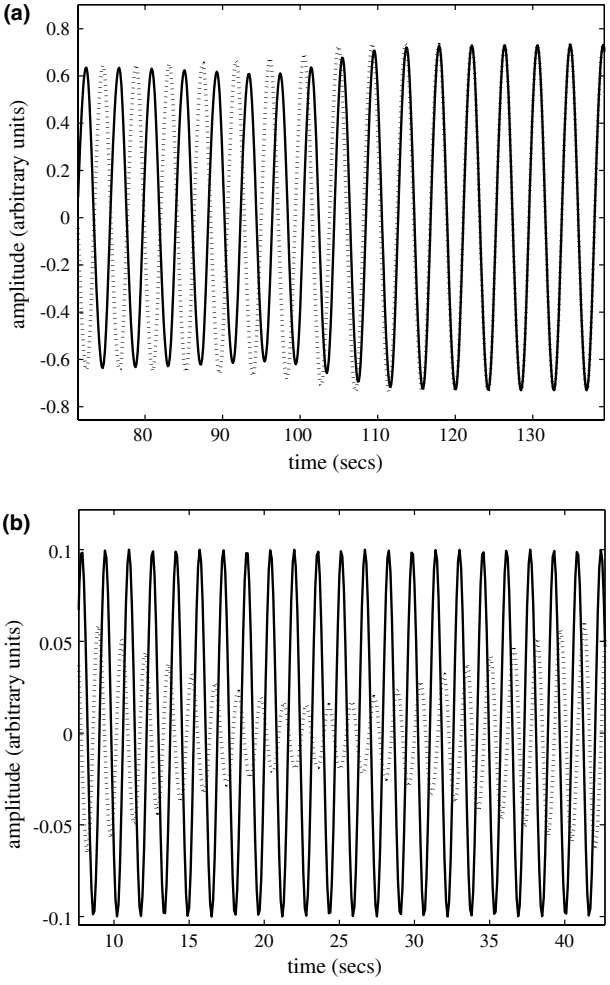

Fig. 13 Two kind of phase transitions. **a** Time series of a coupled oscillator system showing a phase-mediated transition. The trajectories are obtained by integrating the HKB model (equations 1, 2, and 3). The transition takes place over a few cycles without a significant change in the amplitude of the oscillation. The *solid* and the *dotted lines* are the time series of each oscillator of the coupled oscillator system. **b** Time series of a parametrically driven oscillator given by (9) showing an amplitude-mediated transition

in the opposite phase. With this general description of phase transitions in hand, let us now examine the kind of transitions observed in our model. The equations of motion for the complete system are given by Eqs. (19, 20). Here, we consider only the single metronome condition, that is, the frequency of finger movement coincides with that of the metronome. In the $\dot{\phi}$ equations, we notice contributions due to linear and parametric driving terms. A parametric driving term leads to bistability, that is, there are two stable fixed points in the phase space of the system and depending on initial conditions the system tends towards one of the fixed points. Linear driving enforces monostability in the system by destabilizing one of the fixed points. The state of the system, monostability or bistability, is determined by the relative contributions of the two terms. From Eq. (20), we can see that the amplitude plays a crucial part in the transition. The contribution from

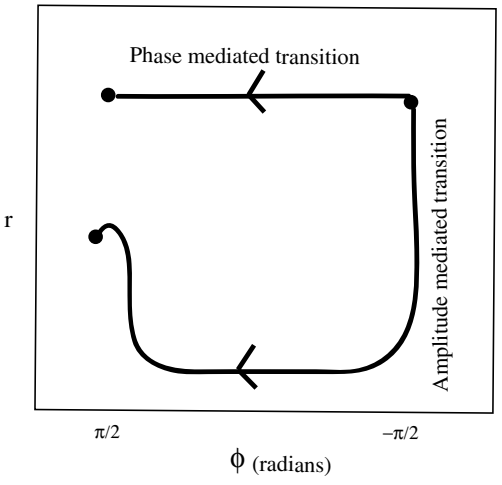

Fig. 14 Two mechanisms of phase transitions in rhythmic coordination, an amplitude- and a phase-mediated transition in the plane spanned by the amplitude, r, and the phase, ϕ

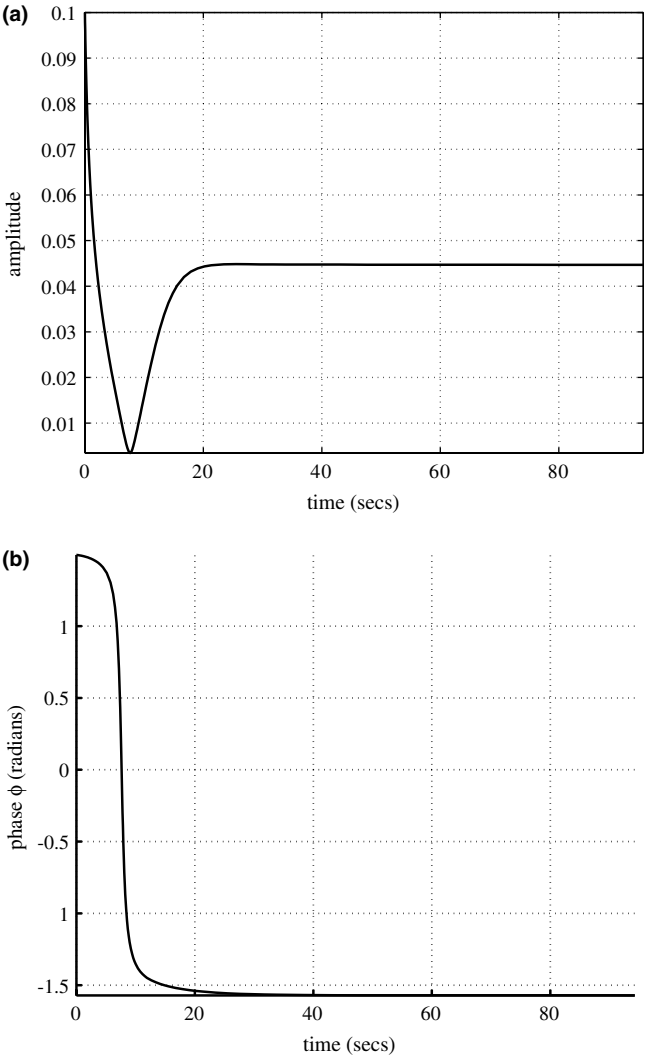

Fig. 15 Plot of the time series of the amplitude, r, (**a**) and the phase, ϕ, (**b**) during an amplitude-mediated transition obtained by simulating equations (19) and (20). A drop in the amplitude is accompanied by a jump in the phase through an angle π. A = 1.5; B = 1; $\gamma = 1$; $\epsilon_1 = 0.1$; $\epsilon_2 = 3$; $\omega = 2$

the linear driving term depends inversely on the amplitude. As the amplitude of the oscillator approaches zero, this contribution far outstrips that of the parametric driving term and the system becomes monostable. The local dynamics in the vicinity of a transition can be classified as an amplitude-mediated transition. In Figs. 15a and 15b, we numerically integrated Eqs. (19) and (20) to obtain the time series of the amplitude and the phase of the complete system. Coincident with the drop in amplitude (Fig. 15a), the time series of the phase (Fig. 15b) shows a transition $\pi/2$ to $-\pi/2$.

Due to the presence of the $1/r$ term in the phase equation, we cannot adiabatically eliminate the phase for the entire time course. However, in the neighborhood of a phase transition the trajectory in the r vs ϕ space does not show any change in the direction of the phase variable, i.e. $\dot{\phi} = 0$. Figures 16a–c describe the dynamics of the system in the $r - \phi$ plane. Consider the set of points with $\dot{r} = 0$. These are called the r nullcline. The set of points with $\dot{\phi} = 0$ are called the ϕ nullcline. The arrows shown in Figs. 16a–c point in the direction of the flow of the vector field given by Eqs. (19, 20). At points on the r nullcline, the r component of the flow is zero, that is, the arrows point in the horizontal direction. At points on the ϕ nullcline, the ϕ component of the flow is zero, that is, the arrows point in the vertical direction. The intersections of the r and the ϕ nullclines are the fixed points of the system.

Figures 16a–c show the nullclines and the flow directions in the $r - \phi$ plane for different values of the strength of the linear driver, ϵ_1. As mentioned earlier, the relative contributions of linear, ϵ_1, and parametric, ϵ_2, driving terms determine the monostability or bistability of the system. In Fig. 16a, $\epsilon_1 = 0.05$. Here, the contribution due to the linear driving term is negligible and the system shows the presence of three fixed points, two stable and one unstable. As ϵ_1 is increased to 0.1 in Fig. 16c, one of the stable fixed points and the unstable fixed point coalesce and disappear and all the trajectories converge to the remaining stable fixed point, that is, the system becomes monostable. Preliminary data from DeGuzman et al. (2002) provide some confirmation of an amplitude-mediated transition mechanism for the case of bimanual coordination. The experiment compared data from two experimental paradigms, that is, coordination of cyclical finger movements with and without a metronome. DeGuzman et al. (2002) report that in the presence of an external metronome subjects perform a transition from anti-phase to in-phase coordination states via an amplitude-mediated mechanism in 70% of all trials examined. In contrast, in the self-paced case, that is, coordination in the absence of a metronome, subjects showed phase-mediated transitions in about 80% of the trials examined. The self-paced case can be clearly described using the original HKB equations. However, in order to describe the results for the metronome-paced case, one would require the presence of a linear and a parametric driving term.

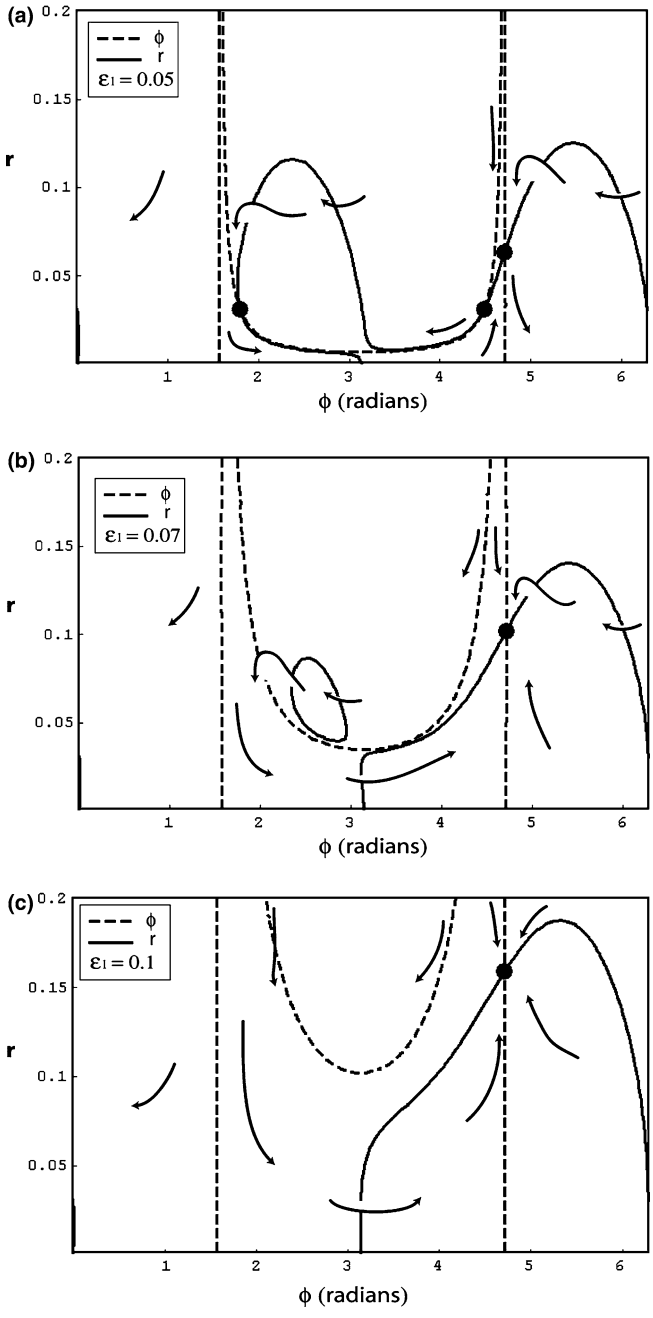

Fig. 16 Plots of the amplitude, r, and the phase, ϕ, as a function of increasing the strength of the linear coupling, ϵ_1, showing the mechanism of an amplitude-mediated transition for (19, 20). The *solid dots* represent the fixed points of the system. The *arrows* show the approximate direction of the flow in the space spanned by the amplitude, r, and the phase, ϕ. See text for details

7 Summary and conclusions

The chief motivation behind this study was to examine the nature of action-perception coupling in the coordination dynamics of movement. Rhythmic movements, driven by a periodic stimulus, present a paradigm that is ubiquitous in nature and has the additional advantage of being accessible in terms of well-studied ideas of oscillator theory. Numerous experimental and theoretical studies have demonstrated the appositeness of this approach. We employed a limit cycle oscillator, based on the Haken–Kelso–Bunz model, to describe the intrinsic dynamics of the system. The external metronome was operationalized by a periodic external stimulus. Our central hypothesis was that the coupling between the external metronome and the intrinsic dynamics of the system cannot be described by a purely linear driver. Therefore, a minimal description of the system must use a parametric driving term. Here, we described an experimental strategy to verify this hypothesis. Parametrically driven limit cycle oscillators are characterized by the presence of Arnol'd tongue structures (as shown in Fig. 1). The experiment consisted of driving the system through different regions of the parameter space to extract signatures of the Arnol'd tongue structures using frequency, amplitude, and phase measures. The synchronization behavior exhibited by subjects clearly showed the presence of 1:1 and 1:2 coordination regimes. Signatures of the 1:1 and 1:2 Arnol'd tongue structures were also seen in the reduced standard deviation of the phase associated with these regions (Sect. 5.3). Experimentally observed anchoring phenomena were shown to be a consequence of parametrically driving the limit cycle oscillator. The model presented accounts for bistability, and a transition from bistability to monostability as observed in unimanual coordination experiments. The main new feature of our theoretical model is the existence of two mechanisms via which a phase transition can be achieved, an amplitude-mediated transition and a phase-mediated transition. The transitions follow mutually orthogonal paths to a steady state. A possible quantification of the degree of phase or amplitude mediation can be described by examining the movement trajectories in the space spanned by the amplitude and phase of finger movement. Before a transition, the fluctuations in the direction of the slower variable should be significantly lower than that of the fast variable. This prediction is now open to further experimental tests.

References

Beek PJ, Peper CE, Daffertshofer A (2002) Modeling rhythmic interlimb coordination: Beyond the haken-kelso-bunz model. Brain Cogn 48:149–165

Buck J, Buck E (1976) Synchronous fireflies. Sci Am 234:74–85

Byblow WD, Carson RG, Goodman D (1994) Expressions of asymmetries and anchoring in bimanual coordination. Hum Mov Sci 13:3–28

Collins JJ, Stewart IN (1993) Coupled nonlinear oscillators and the symmetries of animal gaits. J Nonlinear Sci 3:349–392

DeGuzman GC, Jirsa VK, Assisi CG, Kelso JAS (2002) Phase and amplitude-mediated transitions in coordination phenomena. Society for Neuroscience. 2002 Abstract Viewer/Iternary Planner

DeGuzman GC, Kelso JAS (1991) Multifrequency behavioral patterns and the phase attractive circle map. Biol Cybern 64:485–495

Fink PW, Foo P, Jirsa VK, Kelso JAS (2000) Local and global stabilization of coordination by sensory information. Exp Brain Res 134:9–20

Grossberg S, Pribe C, Cohen MA (1997) Neural control of interlimb oscillations. Biol Cybern 77(2):131–140

Haken H (1983) Synergetics: an introduction 3 edn. Springer Series in Synergetics. Springer, Berlin Heidelberg New York

Haken H, Kelso JAS, Bunz H (1985) A theoretical model of phase transitions in human hand movements. Bio Cybern 51:347–356
Haken H, Peper CE, Beek PJ, Daffertshofer A (1996) A model for phase transitions in human hand movements during multifrequency tapping. Physica D 90:179–196
Jirsa VK, Fink P, Foo P, Kelso JAS (2000) Parametric stabilization of bimanual coordination: A theoretical model. J Bio Phys 1:85–112
Jirsa VK, Haken H (1997) A derivation of a macroscopic field theory of the brain from quasi-microscopic neural dynamics. Physica D 99:503–526
Kay BA, Kelso JAS, Saltzman EL, Schöner G (1987) Steady state and perturbed rhythmical movements: A dynamical analysis. J Exp Psychol Hum Percep Performance 17:183–197
Kay BA, Warren WH J (1998) A dynamical model of coupling between posture and gait. In Rosenbaum DA, Collyer CA (eds) Timing Behavior MIT, Cambridge
Kay BA, Warren WH (2001) Coupling of posture and gait: Mode locking and parametric excitation. Bio Cybern 85:89–106
Kelso JAS (1984) Phase transitions and critical behavior in human bimanual coordination. Am J Physiol Regul Integr Comp 15:R1000–R1004
Kelso JAS, Bressler SL, Buchanan S, Deguzman GC, Ding M, Fuchs A, Holroyd T (1992) A phase-transition in human brain and behavior. Phys Lett A 169(3):134–144
Kelso JAS, DeGuzman GC, Holroyd T (1991) Rhythms in physiological systems, vol 55. Springer Series in Synergetics, chapter Synergetic dynamics of biological coordination with special reference to phase attraction and intermittency. Springer, Berlin Heidelberg New York, pp 195–213
Kelso JAS, DelColle JD, Schöner G (1990) Attention and performance XIII, chapter Action-perception as a pattern formation process, Erlbaum, Hillsdale, pp 136–169
Kelso JAS, Fuchs A, Jirsa VK (1999) Analysis of neurophysiological brain functioning, chapter Traversing scales of organization I: Concepts and experiments, Springer series in synergetics. Springer, Berlin Heidelberg New York, pp 73–89
Kelso JAS, Holt KG (1980) Exploring a vibratory systems-analysis of human movement production. J Neurophysiol 45(5):1183–1196
Kelso JAS, Holt KG, Rubin P, Kugler PN (1981) Patterns of human interlimb coordination emerge from the properties of nonlinear limit cycle oscillatory processes: theory and data. J Mot Behav 13:226–261
Kelso JAS, Scholz JP, Schöner G (1986) Nonequilibrium phase transitions in coordinated biological motion: Critical fluctuations. Phys Lett A 118:279–284
Kugler PN, Turvey MT (1997) Information, natural law, and the self-assembly of rhythmic movement. Lawrence Erlbaum Associates, Inc Hillsdale
Mayville JM, Fuchs A, Ding M, Cheyne D, Deecke L, Kelso JAS (2001) Event-related changes in neuromagnetic activity associated with syncopation and synchronization timing tasks. Hum Brain Mapp 14:65–80
Nagashino H, Kelso JAS (1992) Phase transitions in oscillatory neural networks. Science of Artificial Neural Netw SPIE 1710:278–297
Peper CE, Beek PJ, Van Wieringen PCW (1995) Frequency induced phase transitions in bimanual tapping. Biol Cybern 73(4):301–309
Scholz J, Kelso JAS, Schöner G (1987) Nonequilibrium phase transitions in coordinated biological motion: critical slowing down and switching time. Phys Lett A 123:390–394
Schöner G, Haken H, Kelso JAS (1986) A stochastic theory of phase transitions in human hand movements. Biol Cybern 53:247–257
Schöner G, Jiang WY, Kelso JAS (1990) A synergetic theory of quadrupedal gaits and gait transitions. J Theor Biol 142(3):359–391
Schöner G, Kelso JAS (1988a) Dynamic pattern generation in behavioral and neural systems. Science 239:1513–1520
Schöner G, Kelso JAS (1988b) A synergetic theory of environmentally-specified and learned patterns of movement coordination: Ii. component oscillator dynamics. Biol Cybern 58:81–89
Schöner G, Kelso JAS (1988c) A synergetic theory of environmentally-specified and learned patterns of movement coordination:i. relative phase dynamics. Biol Cybern 58:71–80
Treffner PJ, Turvey MT (1996) Symmetry, broken symmetry, and handedness in bimanual coordination dynamics. Exp Brain Res 107(3):463–478
Yamanishi J, Kawato M, Suzuki S (1980) Two coupled oscillators as a model for the coordinated finger tapping by both hands. Biol Cybern 37:219–225
Yuasa H, Ito M (1990) Coordination of many oscillators and generation of locomotry patterns. Biol Cybern 63:177–184